First-principles study of a Mn-doped In_2Se_3 monolayer: Coexistence of ferromagnetism and ferroelectricity with robust half-metallicity and enhanced polarization

Chunmei Zhang,[1,2,*] Lei Zhang,[1] Cheng Tang,[1] Stefano Sanvito,[3] Bo Zhou,[2] Zhenyi Jiang,[2] and Aijun Du[1,*]

[1]*Centre for Materials Science, School of Chemistry and Physics, Science and Engineering Faculty, Queensland University of Technology, Gardens Point Campus, Brisbane QLD 4001, Australia*

[2]*Institute of Modern Physics, School of Physics, Northwest University, Xi'an 710069, People's Republic of China*

[3]*School of Physics and CRANN Institute, Trinity College, Dublin 2, Ireland*

(Received 15 November 2019; revised 13 September 2020; accepted 21 September 2020; published 13 October 2020)

Two-dimensional (2D) materials with coexistence of ferromagnetism (FM) and ferroelectricity (FE) are rare. By using first-principles modeling, here we report that doping of magnetic transition metal (TM) atoms in FE monolayer In_2Se_3 could introduce giant local FM magnetic moments (4 μ_B per Mn atom). The exchange splitting energy, and the C_{3v} crystal field together with the hybridization of the Mn-d and Se-p orbitals result in spin-polarized states near the Fermi surface. More interestingly, the asymmetric charge distribution of the Jahn-Teller ion (Mn^{3+} d^4) further lift the twofold degeneracy of the Mn-d $e1^*$ states. This affects the band structure and enhances the FE polarization in monolayer In_2Se_3. Our work paves the way for tailoring FM in 2D FE via doping magnetic moments from TM atoms. The half-metallicity combined with the enhanced FE polarization make Mn-doped In_2Se_3 a candidate for potential applications in information technology and spintronic devices.

DOI: 10.1103/PhysRevB.102.134416

I. INTRODUCTION

Two-dimensional (2D) ferromagnetic (FM) and ferroelectric (FE) materials may define applications in information technology and spintronics. Both the FM magnetization and the FE polarization can encode information, which can be read by a magnetic and an electrical field, respectively. Thus, this materials class has recently attracted intensive research interest. Although a few 2D FM materials have been successfully exfoliated in experiments, namely $Cr_2Ge_2Te_6$ [1], CrI_3 [2], Fe_3GeTe_2 [3], VSe_2 [4], their controlled growth and characterization still remain challenging. In fact, most of them are highly unstable in air [5], a fact that hinders their use in practical applications. Out-of-plane FE materials appear especially important, since the out-of-plane FE polarization direction is technologically relevant for the integration of thin film technology [6]. Until now, examples of experimentally fabricated out-of-plane FE compounds, down to one-monolayer thickness, are only limited to $BiFeO_3$ [7] and α-In_2Se_3 [6,8].

At present, special attention has been dedicated to materials that combine FE and FM properties [9,10], as these are ideal candidates to realize electric-write/magnetic-read memory devices, which are expected to have a space in the future circuit design of next-generation nanodevices [11]. In order to achieve ferromagnetism and ferroelectricity simultaneously in 2D, some theoretical approaches have been proposed including: charging $CrBr_3$ monolayer [9], CrI_3/Sc_2CO_2 heterostructures [12], and ($Ti_{0.8}Co_{0.2}O_2/Ca_2Nb_3O_{10}/Ti_{0.8}Co_{0.2}O_2$) superlattices [13]. However, given that only very few 2D FE and FM materials have been synthesized, none of these proposed structures exists in nature or has been fabricated. Moreover, transition metal (TM) d electrons, which are essential for magnetism, often fail to offer off-center FE distortion [14]. Thus, the coexistence of FM and FE is rarely met in a single layer.

Fortunately, the use of TM impurities as spin dopants in semiconductors is at a quite mature stage both theoretically and experimentally [15,16]. Here TM atoms provide the source of spins and sometime free charges in otherwise nonmagnetic semiconductors. Examples include TM-doped TiO_2 [17], GaAs [18], and ZnO [19]. In addition, often the exchange interaction between the TM dopants and free carriers (the sp-d exchange interaction) in a magnetic semiconductor [20] results in magnetic, as well as optical and conductive properties. Therefore, one can also attempt at developing a material where ferromagnetism and ferroelectricity coexist by doping a FE compound with magnetic TM ions. Materials with out-of-plane FE polarization, namely $BiFeO_3$ [7] and α-In_2Se_3 [6,21], are target materials due to their potential technological application. The origin of the FE behavior in $BiFeO_3$ and in α-In_2Se_3 is sharply different. The FE transition in perovskite oxides, like $BiFeO_3$, is generally attributed to small uniaxial atomic distortions (~10 pm), whereas in monolayer In_2Se_3, the asymmetric Se atoms in the middle of the layer spontaneously breaks the centrosymmetry, leading to two energetically degenerate states with opposite (up/down) out-of-plane electric polarization. Such a type of out-of-plane locking arising from the unique covalent bond configuration [22] ensures a strong resilience of the out-of-plane polarization against depolarization fields. Thus α-In_2Se_3 is particularly attractive due to the highly stable out-of-plane polarization at room temperature [6,21]. Ferroelectricity and ferromagnetism will then have a good chance to coexist, if ferromagnetism can be introduced via doping TM atoms in a monolayer α-In_2Se_3.

*Corresponding authors: chunmeizhang@nwu.edu.cn; aijun.du@qut.edu.au

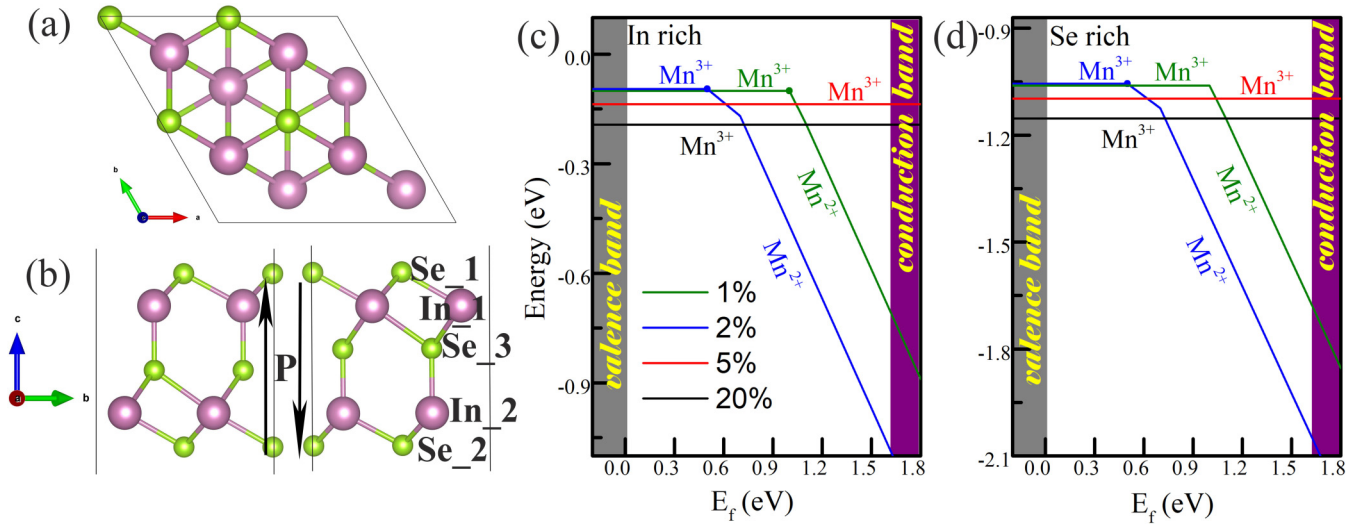

FIG. 1. (a), (b) top and side views (with opposite polarizations – black arrow) of 2×2×1 supercell for an In_2Se_3 monolayer. (c), (d) Calculated formation energies of the most favorable charge states of Mn_{In1} in In_2Se_3 monolayer as a function of the Fermi energy in In-rich and Se-rich growth conditions based on HSE method. Black, red, blue, green line represent 20%, 5%, 2%, 1% Mn-doped In_2Se_3, respectively.

In this work we study, by using density functional theory (DFT), Mn-doping in an In_2Se_3 monolayer with the goal of demonstrating the coexistence of a spontaneous magnetization and an out-of-plane electric polarization. Mn *d* electrons exhibit high spin configuration ($4\,\mu_B$) when doped in In_2Se_3 as the exchange splitting energy outweighs the C_{3v} crystal field splitting energy. Mn doping induces half-metallicity in In_2Se_3 monolayer and leads to a Mn d^4 asymmetry configuration associated to Jahn-Teller distortion, which splits the Mn-*d* e1* states. The Jahn-Teller distortion competes with the Mn-Mn interaction and a lower symmetry is expected at low Mn concentrations. This is consistent with the results that a more enhanced polarization is observed at a lower Mn doping concentration in In_2Se_3 monolayer.

II. COMPUTATIONAL DETAILS

Geometry relaxation was performed using DFT within the generalized gradient approximation (GGA) of Perdew, Burke, and Ernzerhof (PBE) of the exchange and correlation energy functional [23], as implemented in the Vienna *ab initio* simulation package (VASP) [24,25]. The hybrid functional from Heyd, Scuseria, and Ernzerhof (HSE) [26] was adopted to search for the magnetic ground state and accurately calculate the band structure. Long-range van der Waals interactions (DFT-D3 method) were incorporated to correct the total energy [27]. A vacuum layer with a thickness of more than 10 Å is used to minimize the artificial interactions between the layer periodic replicas. In order to guarantee the convergence of the calculated electropotential energy, a test on the thickness of the vacuum layer have been undertaken. Thicknesses of 13.5 Å for 2%, 5%, 20% Mn doping and 17.5 Å for 1% Mn-doped In_2Se_3 are adopted. An energy cutoff of 500 eV is set for the plane-wave basis set. The geometry of the Mn-doped In_2Se_3 monolayer has been fully optimized until the energy and the forces converge within 10^{-6} eV and 0.001 eV/Å, respectively. To simulate different Mn concentrations, we build 4×4×1, 3×3×1, 2×2×1, and 1×1×1 supercells of the In_2Se_3 monolayer with 1 Mn dopant, corresponding to Mn concentrations of 1%, 2%, 5%, and 20%, respectively. The Brillouin zone integration was sampled by 1×1×1, 2×2×1, 4×4×1, 7×7×1, 7×7×1 *k*-grid meshes for 1%, 2%, 5%, 20%, 0% Mn-doped In_2Se_3 monolayers, respectively. Spin-orbit-coupling (SOC) was also included in the calculation. The out-of-plane electric polarization of Mn-doped In_2Se_3 was obtained with the classical electrodynamic method by direct integrating $\rho * z$ over the entire supercell, where ρ is the local charge density and z is the coordinate along the out-of-plane axis [6]. And the polarization value is the difference between the up and down states. *Ab initio* molecular dynamics (AIMD) simulations with canonical ensemble were performed to evaluate the thermodynamic stability.

III. RESULTS AND DISCUSSION

A. The most favorable growth conditions for Mn doping in In_2Se_3 monolayer

In_2Se_3 monolayer belongs to the P3m1 space group with C_{3v} symmetry as shown in Figs. 1(a) and 1(b); In and Se atoms, forming a honeycomb structure, stacked alternately along the *c* axis. Figure 1(b) presents two configurations with the out-of-plane electric polarization pointing upward (left) and downward (right). When Mn is introduced in In_2Se_3 structure, three doping sites can be considered: substitutional for In (Mn_{In}), substitutional for Se (Mn_{Se}), or interstitial (Mn_I). The formation energies of the different doping sites at different concentrations are computed based on the following equation [28] and compared in Table s1 of the Supplemental Material [29]:

$$E_{form}(\mathrm{Mn}) = E_{tot}(\mathrm{Mn}) - E_{tot}(\mathrm{In_2Se_3}) - \sum_i n_i\mu_i. \quad (1)$$

Here $E_{tot}(\mathrm{Mn})$ and $E_{tot}(\mathrm{In_2Se_3})$ are the total energies of a supercell containing one Mn impurity and of an identical supercell containing only the host In_2Se_3 layer, respectively. The

chemical potential for the ith species is μ_i, and n_i indicates the number of atoms that have been added to or removed from the supercell. The values of μ_i are subject to constraints imposed by the experimental growth conditions (for calculation details see the Supplemental Material [29]). The calculated formation energies of Mn-doped In_2Se_3 (see Table S1 and Fig. S1 in the Supplemental Material [29]) indicate that the In_1 substitutional sites (Mn_{In1}) are the most energetically favorable. This may be expected, since the ionic radius of Mn atom is Mn^{3+} 64.5 pm [30], which is rather close to that of In^{3+} 62 pm.

In the above calculations the entire cell is kept charge neutral. The Mn impurities might hold a 3+ charge state, like that of Mn_{In1} in In_2Se_3. Therefore, we further study the formation energies of the doped Mn impurities in various charge states. In this case, the formation energy of the charged impurity is defined as [28]

$$E_{\text{form}}(\text{Mn},\ q) = E_{\text{tot}}(\text{Mn},\ q) - E_{\text{tot}}(\text{In}_2\text{Se}_3) - \sum_i n_i\mu_i + q(E_f + E_v + \Delta V), \quad (2)$$

where $E_{\text{tot}}(\text{Mn},\ q)$ is the total energy of a supercell containing one Mn impurity in the charge state q and E_f is the Fermi energy with respect to the valence band maximum (VBM) of the In_2Se_3 monolayer (E_v). In Eq. (2) ΔV is a potential alignment due to the different energy reference among the defected and the pristine supercell.

Figures 1(c) and 1(d) show the calculated formation energies of the Mn impurities in their favorable charge states as a function of Fermi surface in In- and Se-rich growth conditions based on the HSE functional, respectively. The formation energies of Mn^{3+} and Mn^{2+} are much lower in Se-rich condition compared to the In-rich condition [Figs. 1(c) and 1(d)]. Thus, Se-rich conditions are more favorable than In-rich ones for doping Mn in monolayer In_2Se_3, which agrees with the experimental result that the growth condition of monolayer In_2Se_3 is Se-rich [31,32]. In a Se-rich environment, the Mn^{3+} state is always preserved over the entire Mn concentration range. It is only in extreme n-type conditions, when the Fermi energy approaches the conduction band minimum, that the charge state transforms to Mn^{2+} for 1% and 2% Mn concentration, where, Mn^{2+} states have rather negative formation energies. PBE predicts the same trend as HSE (see Fig. S2 in the Supplemental Material [29]).

B. Magnetic ground state and band structure for Mn doped In_2Se_3 monolayer

Having identified the most favorable growth conditions for Mn doping in In_2Se_3, we now analyse the structures and the ground-state spin-configuration of such Mn-doped systems. In particular we consider various Mn concentrations, ranging from 1% to 20% (Fig. S3 in the Supplemental Material [29]). A further AIMD calculation demonstrates that the asymmetric structures of monolayer In_2Se_3 with partial In-to-Mn substitution remain intact above room temperature, while there is a asymmetric-to-symmetric phase transition when all the In atoms are replaced by Mn, namely for the Mn_2Se_3 monolayer under 500 K (see Fig. S4b in the Supplemental Material [29]). Each Mn impurity has seven valence electrons, so that the Mn^{3+} charge state is generally encountered. The occupied Mn^{3+} state, with four d electrons, can exhibit either a high-spin configuration ($d^4{}_\uparrow d^0{}_\downarrow$ with a magnetic moment (MM) of $4\,\mu_B$), or a low-spin configuration ($d^3{}_\uparrow d^1{}_\downarrow$ with MM of $2\,\mu_B$), or a nonmagnetic configuration ($d^2{}_\uparrow d^2{}_\downarrow$ with MM $0\,\mu_B$). These are determined by the relative energy of the crystal field and the exchange splitting. The calculated PBE and HSE results shown in Table S2 in the Supplemental Material [29] demonstrate that the $d^4{}_\uparrow d^0{}_\downarrow$ configuration is the ground state of Mn-doped In_2Se_3 monolayer, meaning that the exchange splitting energy is larger than that of the crystal field. Both PBE and HSE results show that d electrons are fully polarized and the predicted MM is $4\,\mu_B$/Mn, which is the largest among all the $3d$ TM metals (Table S3 in the Supplemental Material [29]).

In order to identify the magnetic ground state, various possible magnetic orders are compared within a $2\times2\times1$ supercell relative to 1%, 2%, 5%, and 20% Mn concentrations in which 4 Mn atoms are included. These include nonmagnetic (zero local moments), FM (↑↑↑↑), antiferromagnetic (↑↑↓↓), and ferrimagnetic (↑↑↑↓) [33] and their energies are compared in Table S4 in the Supplemental Material [29]. It is confirmed that the FM state has the lowest energy for Mn-doped In_2Se_3 at doping concentrations varying from 1% to 20%. Given the FM ground state, the spin-polarized electronic properties of pure and Mn-doped In_2Se_3 monolayers are also calculated by both GGA-DFT and hybrid functional. The bandgap of n-type monolayer In_2Se_3 are 1.59 eV [Fig. 2(a)] and 0.63 eV (Supplemental Material [29] Fig. S5a) for HSE and PBE, respectively. HSE predicts a nearly zero bandgap for spin up and band gaps of 1.51, 1.15, 1.65, 2.36 eV for spin down of 1%, 2%, 5%, and 20% Mn concentration, respectively [Figs. 2(b)–2(e)]. The 1% Mn-doped In_2Se_3 are only calculated along Γ-K-M-Γ due to the computing demanding. This suggests that the material may be half metallic [34] for large Mn concentrations, while it remains insulating at low doping levels. Note, however, that despite the fact that the exchange interaction is strong, a long-range magnetic order for such diluted system will develop only if the concentration of the Mn ions exceed the percolation threshold [34]. For the 2D hexagonal lattice and nearest neighbor interaction this is of the order of 0.7, but it can be reduced, as the range of the magnetic interaction gets longer. Note also that a long-range interaction is needed to overcome the Wagner-Mermin theorem. To help to lift the Wagner-Mermin restriction, magnetocrystalline anisotropy energy (MAE) is especially important for 2D magnetic materials, allowing the long-range FM order to survive at finite temperature even in the monolayer limit [1]. We calculated the MAE energy for 5% Mn-doped In_2Se_3 for example (more details in the Supplemental Material [29]), the out-of-plane magnetic anisotropy is preferred and the calculated MAE energy is ∼1.503 meV, which is significantly larger than the value for many FM monolayers, such as ∼0.100 meV for $Cr_2Ge_2Te_6$ [35], 0.920 meV for Fe_3GeTe_2 [36], 0.804 meV for CrI_3 [37]. Importantly, even if a macroscopic magnetic order does not develop, one can still observe in these diluted systems local magnetism. Thus, Mn-doped In_2Se_3 materials could find possible applications in high-density magnetic data storage.

In a C_{3v} crystal field, the Mn^{3+} $3d$ orbitals should be split into e1 (d_{xy}, $d_{x^2-y^2}$), $e1^*$ (d_{xz}, d_{yz}), and $a1$ (d_{z^2}) states. As the crystal splitting energy is lower than the exchange splitting

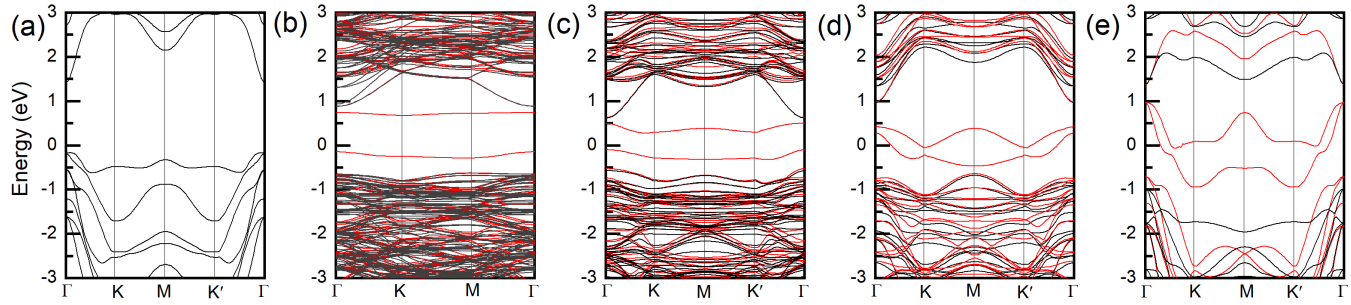

FIG. 2. The band structure of (a) In_2Se_3 monolayer, (b) 1%, (c) 2%, (d) 5%, and (e) 20% Mn-doped In_2Se_3 monolayer calculated by HSE method. Note that different Mn doping concentration corresponds to different supercells, which is described in the calculation method. The red and black lines represent the band structure composed by spin-up and spin-down electrons. The Fermi surface is shifted to 0 eV.

for Mn-doped In_2Se_3 monolayer, Mn will keep a high-spin configuration, where the spin-up d states are mostly occupied and the spin-down d states remain completely empty (Fig. S6 in the Supplemental Material [29]). The spin-up Mn d $e1^*$ state has a Se p projection due to hybridization. The strong d-p coupling results in a high crystal field splitting, pushing the occupied Mn $e1^*$ states to a higher energy. A detailed analysis of the 5% doping case shows that Mn d $e1^*$ states can only couple with its neighboring Se p orbitals. Thus, the Mn $e1^*$ states merge into the VBM of the host In_2Se_3 through its hybridization with neighboring Se atoms (more explanation see the Supplemental Material and Fig. S7 [29]). SOC effects are also investigated. However, the main contribution to the Fermi surface is from the Se p orbitals and the effect of SOC remains negligible, as shown in Fig. S8 in the Supplemental Material [29].

C. Jahn-Teller distortion

Because of the C_{3v} symmetry, the d_{xz}, d_{yz} orbitals should be energetically degenerate at the Γ point. However, a detailed analysis around the Γ point in Fig. 3 shows that the energy of d_{xz} is higher than that of d_{yz}, thus a further analysis of the d orbitals is needed. The Mn^{3+} ion has a d^4 configuration, which means that the d shell is partially filled with one empty orbital. As a result, Mn^{3+} becomes Jahn-Teller unstable [38]. In addition, degenerate electronic states occupying the $e1^*$ orbital in general tend to show stronger Jahn-Teller distortion due to the occupation of high energy orbitals. Since the system is more stable with a lower energy configuration, the degeneracy of the $e1^*$ set is broken, and the symmetry is reduced. Hence, one of the $e1^*$ degenerate orbitals will move to a lower energy (Mn d_{yz}) and the other to a higher one (Mn d_{xz}). Thus, we infer that this further large orbital splitting [Figs. 3(a), 3(c), and 3(e)] is attributed to the Jahn-Teller distortion, which lowers the entire system energy. To prove this point, we analyze charge compensation by doping one electron to fill the Mn d state in Mn-doped In_2Se_3. Figure 3 demonstrates that the orbital splitting for charge compensated Mn d^5 system is greatly reduced and close to zero compared to Mn d^4. However, there is still a small bandgap around 0.127, 0.035, and 0.033 eV for 1%, 2%, 5% Mn-doped In_2Se_3 at the Γ point [Figs. 3(b), 3(d), and 3(f)]. We believe that the origin of such bandgap is that no symmetry is imposed on the system and also there is small amount of the compensated charge spreading over the whole cell instead of being localized at the Mn position. More interestingly, orbital splitting would reduce the Mn-Mn interaction as the hopping between orbitals require further energy, thus the Jahn-Teller distortion would compete with the Mn-Mn interaction. It is also true from our figure that the orbital splitting is smaller at a larger Mn doping concentration. With the Mn concentration getting larger in In_2Se_3, the Mn-Mn interaction dominates over the Jahn-Teller distortion, and the Jahn-Teller effect weakens. A previous finding also supports our idea that a strong Jahn-Teller effect should be observed for lower TM doping concentration [39]. Moreover, a reduced Mn-Mn interaction at small doping concentration decreases the ferromagnetism, which agrees with the relative energies trend between FM and AFM in Table S4 in the Supplemental Material [29].

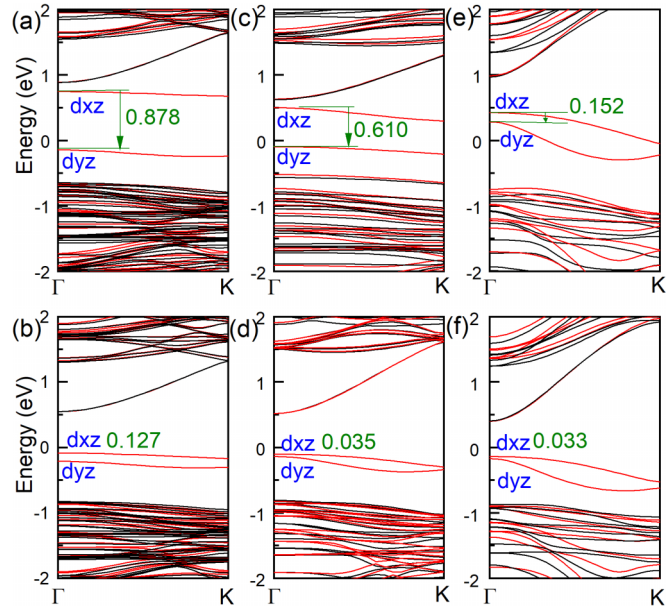

FIG. 3. The band structure along $\Gamma - K$ without charge compensation (Mn d^4) for 1% (a), 2% (c), and 5% (e) for Mn-doped In_2Se_3 system and with charge compensation (Mn d^5) for 1% (b), 2% (d), and 5% (f) for Mn-doped In_2Se_3 system calculated with HSE. The Fermi surface is shifted to 0 eV in (a)–(f).

D. Mn doping induced enhanced electrical polarization

With the orbital splitting getting larger at small Mn doping concentration, a lower symmetry is expected, in line with previous predictions [39]. In this way, the polarization of Mn-doped In_2Se_3 should be influenced by the Mn concentration, having a larger polarization value at a lower doping concentration. In order to prove this conjecture, we further investigate the electrical polarization of Mn-doped In_2Se_3. An out-of-plane polarization would be of technologically relevance for thin-film applications [6]. Mn as dopant in In_2Se_3 would induce further structure asymmetry. Considering that the Jahn-Teller distortion in the *d* shell may alter the electrical polarization of Mn-doped In_2Se_3, we then turn our attention to study the out-of-plane polarization of In_2Se_3 upon Mn doping. The FE polarization of the monolayer In_2Se_3 has been well studied both experimentally and theoretically, having a value of 0.11 eÅ/unit cell [6] or 0.15×10^{-10} C/m [40] along the out-of-plane direction. Our work estimates the polarization of monolayer In_2Se_3 being 0.14 eÅ/unit cell or 0.15×10^{-10} C/m, which is in good agreement with previous work. When Mn is doped into In_2Se_3 monolayer, the polarizations are calculated to be 0.16×10^{-10} C/m, 0.19×10^{-10} C/m, 0.20×10^{-10} C/m, 0.21×10^{-10} C/m for 20%, 5%, 2%, and 1% Mn concentration, respectively. Clearly the polarization is significantly enhanced when Mn is doped, and this gets larger when the concentration is reduced.

IV. CONCLUSIONS

In summary, we have studied the effects of magnetic doping in the FE In_2Se_3 monolayer by using first-principles calculations. Our calculations indicate that the In_1 substitutional site is strongly preferred by Mn^{3+} impurities and that a FM ground state is formed. Mn doping can induce half-metallicity in In_2Se_3 monolayer due to the cooperative Mn pairs exchange interaction and hybridization of the *d* orbital of Mn dopants with the *p*-orbital of neighboring Se atoms at the VBM. Additionally, the Jahn-Teller distortion associated with the Mn $3d^4$ state is significant at a lower Mn doping concentration. Our work delivers a way to realize the coexistence of 2D FM and FE via doping magnetic TM atoms in FE monolayers.

The authors declare no competing financial interest.

ACKNOWLEDGMENTS

A.D. acknowledges the financial support by Australian Research Council under Discovery Project (DP170103598) and computer resources provided by high-performance computer time from computing facility at the Queensland University of Technology, NCI National Facility, and The Pawsey Supercomputing Centre through the National Computational Merit Allocation Scheme supported by the Australian Government and the Government of Western Australia.

[1] B. Huang, G. Clark, E. Navarro-Moratalla, D. R. Klein, R. Cheng, K. L. Seyler, D. Zhong, E. Schmidgall, M. A. McGuire, and D.H. Cobden, Nature (London) **546**, 270 (2017).
[2] C. Gong, L. Li, Z. Li, H. Ji, A. Stern, Y. Xia, T. Cao, W. Bao, C. Wang, and Y. Wang, Nature (London) **546**, 265 (2017).
[3] Y. Deng, Y. Yu, Y. Song, J. Zhang, N.Z. Wang, Z. Sun, Y. Yi, Y.Z. Wu, S. Wu, and J. Zhu, Nature (London) **563**, 94 (2018).
[4] M. Bonilla, S. Kolekar, Y. Ma, H.C. Diaz, V. Kalappattil, R. Das, T. Eggers, H.R. Gutierrez, M.-H. Phan, and M. Batzill, Nat. Nanotechnol. **13**, 289 (2018).
[5] Y. Zhang, J. Chu, L. Yin, T.A. Shifa, Z. Cheng, R. Cheng, F. Wang, Y. Wen, X. Zhan, and Z. Wang, Adv. Mater. **31**, 1900056 (2019).
[6] W. Ding, J. Zhu, Z. Wang, Y. Gao, D. Xiao, Y. Gu, Z. Zhang, and W. Zhu, Nat. Commun. **8**, 14956 (2017).
[7] H. Wang *et al.*, Nat. Commun. **9**, 3319 (2018).
[8] X. Jiang, Y. Feng, K.-Q. Chen, and L.-M. Tang, J. Phys.: Condens. Matter **32**, 105501 (2019).
[9] C. Huang, Y. Du, H. Wu, H. Xiang, K. Deng, and E. Kan, Phys. Rev. Lett. **120**, 147601 (2018).
[10] H. J. Xiang, S. H. Wei, M. H. Whangbo, and J. L. F. DaSilva, Phys. Rev. Lett. **101**, 037209 (2008).
[11] M. Wu and X. C. Zeng, Nano Lett. **16**, 3236 (2016).
[12] Y. Zhao, J. J. Zhang, S. Yuan, and Z. Chen, Adv. Funct. Mater. **29**, 1901420 (2019).
[13] B. W. Li, M. Osada, Y. Ebina, S. Ueda, and T. Sasaki, J. Am. Chem. Soc. **138**, 7621 (2016).
[14] N. A. Hill, J. Phys. Chem. B **104**, 6694 (2000).
[15] J. Xu, J. B. Liu, B. X. Liu, S. N. Li, S. H. Wei, and B. Huang, Adv. Electron. Mater. **4**, 1700553 (2018).
[16] X. Sui, C. Si, B. Shao, X. Zou, J. Wu, B.-L. Gu, and W. Duan, J. Phys. Chem. C **119**, 10059 (2015).
[17] Y. Matsumoto, M. Murakami, T. Shono, T. Hasegawa, T. Fukumura, M. Kawasaki, P. Ahmet, T. Chikyow, S.-Y. Koshihara, and H. Koinuma, Science **291**, 854 (2001).
[18] A. M. Nazmul, T. Amemiya, Y. Shuto, S. Sugahara, and M. Tanaka, Phys. Rev. Lett. **95**, 017201 (2005).
[19] J. R. Neal, A. J. Behan, R. M. Ibrahim, H. J. Blythe, M. Ziese, A. M. Fox, and G. A. Gehring, Phys. Rev. Lett. **96**, 197208 (2006).
[20] P. I. Archer, S. A. Santangelo, and D. R. Gamelin, Nano Lett. **7**, 1037 (2007).
[21] F. Xue, W. Hu, K. C. Lee, L. S. Lu, J. Zhang, H. L. Tang, A. Han, W. T. Hsu, S. Tu, and W. H. Chang, Adv. Funct. Mater. **28**, 1803738 (2018).
[22] J. Xiao, H. Zhu, Y. Wang, W. Feng, Y. Hu, A. Dasgupta, Y. Han, Y. Wang, D. A. Muller, L. W. Martin, P. A. Hu, and X. Zhang, Phys. Rev. Lett. **120**, 227601 (2018).
[23] P. E. Blochl, Phys. Rev. B **50**, 17953 (1994).
[24] G. Kresse and J. Furthmüller, Phys. Rev. B **54**, 11169 (1996).
[25] G. Kresse and J. Hafner, Phys. Rev. B **47**, 558 (1993).
[26] J. Heyd and G. E. Scuseria, J. Chem. Phys. **118**, 8207 (2003).
[27] S. Grimme, J. Comput. Chem. **27**, 1787 (2006).
[28] C. G. Van de Walle and J. Neugebauer, J. Appl. Phys. **95**, 3851 (2004).
[29] See Supplemental Material at http://link.aps.org/supplemental/10.1103/PhysRevB.102.134416 for additional information on the energy comparison between different Mn doping sites, and magnetic states calculated by PBE and HSE methods; TM spin configuration when doped in In_2Se_3 monolayer; calculated

formation energies; the MD simulation of Mn-doped In_2Se_3 monolayer and Mn_2Se_3 monolayer structure changes under 500 K; the band structure of In_2Se_3 monolayer without and with Mn doping by PBE method; magnetocrystalline anisotropy energy calculation details; the orbital resolved band structure for Mn-doped In_2Se_3 monolayer; the band structure of Mn-doped In_2Se_3 monolayer by HSE+SOC method; kinetics pathways of polarization reversal processes for In_2Se_3 monolayer with and without Mn doping; the relationship between doping concentration and polarization value.

[30] C. Amory, N. Guettari, J. Bernède, and M. Mebarki, Phys. Status Solidi **203**, 3726 (2006).

[31] M. Eddrief, C. Julien, M. Balkanski, and K. Kambas, Mater. Lett. **2**, 432 (1984).

[32] J. Zhou, Q. Zeng, D. Lv, L. Sun, and Z. Liu, Nano Lett. **15**, 6400 (2015).

[33] J.-J. Zhang, L. Lin, Y. Zhang, M. Wu, B. I. Yakobson, and S. Dong, J. Am. Chem. Soc. **140**, 9768 (2018).

[34] J. Osorio-Guillén, S. Lany, S. V. Barabash, and A. Zunger, Phys. Rev. B **75**, 184421 (2007).

[35] Y. Fang, S. Wu, Z.-Z. Zhu, and G.-Y. Guo, Phys. Rev. B **98**, 125416 (2018).

[36] H. L. Zhuang, P. R. C. Kent, and R. G. Hennig, Phys. Rev. B **93**, 134407 (2016).

[37] L. Webster and J.-A. Yan, Phys. Rev. B **98**, 144411 (2018).

[38] Y. Yamashita and K. Ueda, Phys. Rev. Lett. **85**, 4960 (2000).

[39] X. Luo and R. M. Martin, Phys. Rev. B **72**, 035212 (2005).

[40] J. Liu and S. Pantelides, 2D Mater. **6**, 025001 (2019).